Viscoelastic Fluid Flow Model for Hydrodynamic Behaviour of Magnetorheological Fluid in Valve and Shear Modes for a Damper System

Adelani Ismail Adeleke
ORCID: https://orcid.org/0000-0003-0837-830X
Department of Mechanical Engineering, Federal University of Agriculture,
Abeokuta, Ogun State, Nigeria
E-mail: adelekeadelani.aasl@gmail.com
Mufutau Adekojo Waheed
ORCID: https://orcid.org/0000-0002-3723-1916
Department of Mechanical Engineering, Federal University of Agriculture,
Abeokuta, Ogun State, Nigeria
E-mail: akindoye@gmail.com
Gbeminiyi Musibau Sobamowo
ORCID: https://orcid.org/0000-0003-2402-1423
Department of Mechanical Engineering, Faculty of Engineering, University of Lagos, Akoka
Lagos, Nigeria
E-mail: gsobamowo@unilag.edu.ng
Antonio Marcos de Oliveira Siqueira
ORCID: https://orcid.org/0000-0001-9334-0394
Federal University of Viçosa, Brazil
E-mail: antonio.siqueira@ufv.br

Abstract

In this present study, the flow behaviour of magnetorheological fluid in valve and shear modes for damping system is modelled and analyzed. The fluid is modelled as viscoelastic fluid flowing between two parallel plates in pressure driven flow mode, and also as direct shear mode. In the work, the post-yield shear thinning or thickening behaviour of magnetorheological fluids are accounted for. The velocity and pressure distributions in the unsteady magnetorheological fluid flow between the electrodes of the damper are obtained by solving the momentum equation of the magnetorheological fluid flow using the Laplace transform method. There is an excellent agreement between the results of the present model and the results of the experimental studies. The adopted viscoelastic flow model describes that the rheological behaviour of the fluid is separated into distinct pre-yield and post-yield regimes. The fluid flow velocity, velocity gradient, and shear stresses have all been shown to be enhanced by an increase in the pressure drop. The viscosity of the fluid increases with an increase in the volume fraction of particles in the fluid, which causes the resistance of the fluid to flow to increase and thereby, reduces the fluid flow velocity. Fluid flow velocity is decreased as a result of increasing magnetic field strength. The design of clutches, rotary brakes, dampers, shock absorbers, prosthetic devices, polishing and grinding tools, etc. will all benefit greatly from the adoption of the current model.

Keywords: Magnetorheological fluid; Viscoelastic fluid; Flow characteristics; Analytical Investigation; Valve mode; Shear Mode; Damper system.

1. Introduction

Magnetorheological fluids are fluids that consist of small particles of iron (in the order of µm) magnetizable, suspended in oil, generally hydrocarbon. Also, some additives are added to the

fluid with objective to inhibit the deposit of iron particles, to promote its suspension, to modify viscosity and to diminish the consuming. One excellent characteristics of magnetorheological fluid is that its rheological characteristics changes when magnetic field is applied. The intensity of applied magnetic field is used to control the viscosity of the fluid. The special behavior of magnetorheological fluid has resulted in its vast of applications such as dampers, shock absorbers, rotary brakes, prosthetic devices, clutches, polishing and grinding devices, etc. Among these applications, magnetorheological fluid dampers, which utilize the advantages of magnetorheological fluids, are semi-active control devices that are widely used in the modern industry nowadays. A typical magnetorheological damper includes MR fluid, a pair of wires, a housing, a piston, a magnetic coil, and an accumulator as shown in Fig. 1. Here, the MR fluid is housed within the cylinder and flows through a small orifice. The magnetic coil is built in the piston or on the housing. When a current is supplied to the coil, the particles are aligned and the fluid changes from the liquid state to the semi-solid state within milliseconds. Consequently, a controllable damping force is produced.
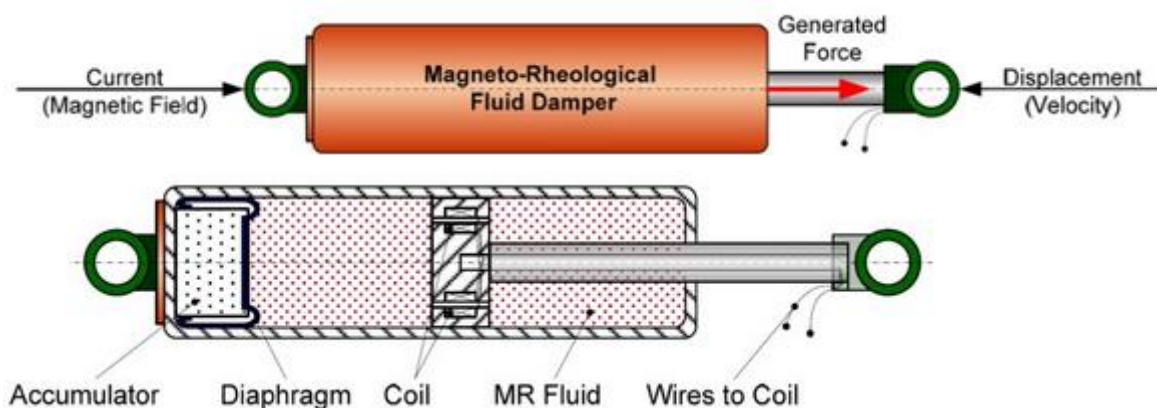

Figure 1. General configuration of a MR fluid damper

The applications of magnetorheological fluids in most devices can be classified as having either fixed plates (pressure-driven flow mode) or relatively moveable plates (direct-shear mode and squeeze-film mode) as shown in Fig. 2b. Examples of pressure-driven flow mode devices include servo-valves, dampers, and shock absorbers and examples of direct-shear mode devices include clutches, brakes, low force dampers, magnetic brakes and clutches chucking and locking devices. The squeeze-film mode of operation also known as biaxial elongational flow mode appears in slow motion and/or high force applications.
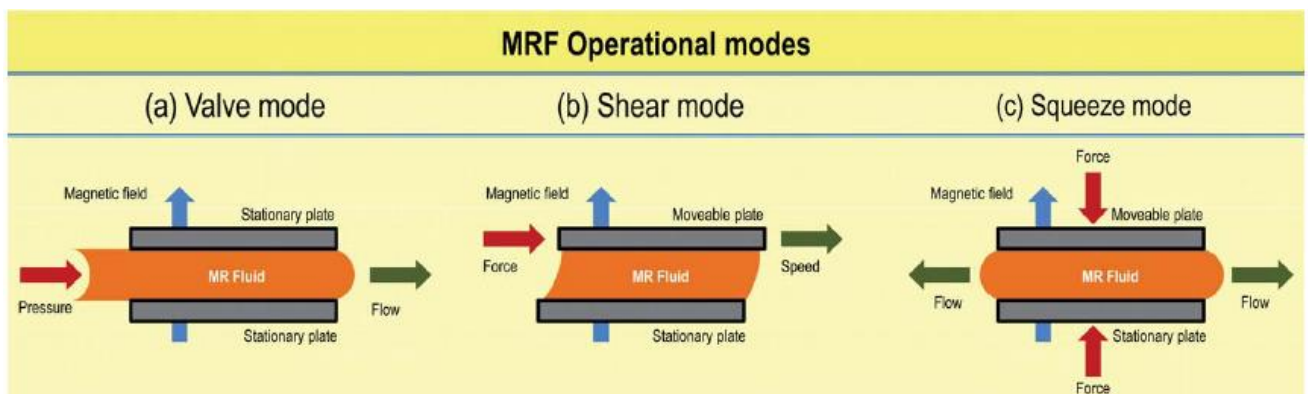

Figure 2. Basic operational modes for controllable magnetorheological fluid devices: (a) pressure driven flow mode, (b) direct shear mode, and (c) biaxial elongational flow mode.

The pressure-driven flow (valve) mode has the magnetorheological fluid in between two fixed magnetic plates. When the magnetic field is applied, magnetorheological particles align parallel to the applied magnetic field lines and resist the flow of the pressurized magnetorheological fluid.

The direct-shear mode has the magnetorheological fluid in between one moving plate and another stationary plate. The relative motion between these plates causes "shearing" in the fluid between the plates. When the magnetic field is applied, magnetorheological particles align perpendicular to the pole plates while the shearing motion attempts to bend the particle chains along the flux lines. As the magnetic field intensity increases, the resistance to shearing offer by the magnetorheological fluid increases. The squeeze-film mode, as the names implies works through squeezing the two magnetic pole plates together on a thin film of magnetorheological fluid. When the force is applied (as shown in Fig. 2) on the plates parallel to the direction of flux lines, it pressurizes the chain-like structures of magnetorheological fluid particles. The intensity of the induced field determines the ability of the magnetorheological fluid particle columns to resist buckling.

The magnetorheological (MR) fluid flow behaviour has been modelled and analyzed. Stepanov *et al*. (2007) explored the impact of a homogeneous magnetic field on the viscoelastic behavior of magnetic elastomers while Chen *et al*. (2019) investigated the slip differential heat of magnetorheological fluids under shear mode operation. Meanwhile, Becnel *et al*. (2012) experimentally investigated the magnetorheological fluid properties at different shear rates. In a previous year, Lindler and Wereley (2003) presented a quasi-steady Bingham plastic analysis of an electrorheological flow mode bypass damper. In the preceding year, Lee *et al*. (2002) utilized Herschel–Bulkley model to analyse the performance of electrorheological and magnetorheological fluids in damper systems. Chen *et al*. (2004) examined the unsteady unidirectional flow of Bingham fluid between parallel plates under different volume flow rate conditions. Wang and Gordaninejad (2007) modelled the flow characteristics of field-controllable, electro-and magneto-rheological fluid dampers. Liao, 2011, studied different parametric models of MR dampers, dynamic models based on Bingham, bi-viscous model and the Bouc-Wen model. Omidbeygi (2012) studied the hydrodynamic properties of an MR fluid in a shear mode inside a rotational eccentric cylinder using the Herschel-Bulkley model. Good fluid consistency was obtained at high shear rates over a wide range of magnetic field strengths. Analytical and numerical comparisons were made to validate these results. Goldasz (2012) analyzed the flow behavior of an MR fluid in a damper using the Bingham, bi-viscous, and Herschel-Bulkley models. The analytical results were compared with the experimental results, and the Herschel-Bulkley model produced results that were more consistent and had a smaller margin of error. In Wang and Gordaninejad's work from 2006, they investigated three magnetorheological fluids at high shear levels. Gedik (2017) presented a comparative study of experimental and numerical methods on magnetorheological fluids in a circular pipe subjected to different magnetic field strengths.

It has been shown that magnetorheological fluid modeling relies on a variety of models, including the Bingham, Herschel-Bulkley, Biviscous, and Hysteretic Biviscous models. These rheological models describe the behavior of MR fluids. Although, the application and mode type affect how MR fluid is modelled, the Bingham and Herschel-Bulkley models are the most widely used due to their simplicity compared to other models. It is more appropriate to use the Herschel-Bulkley model in the case of high values in shear stress However, the Bingham Plastic model is thought to be the most accurate in explaining the relationship between the MR fluid's shear stress and magnetic field. However, Weiss (1994) established the elastic-viscous behaviours of magneto-rheological (MR) fluid and pointed out the viscoelastic properties of Magnetorheological Fluids. Yang *et al*. (2023) provided the magnetorheological and viscoelastic behaviours in an fe-based amorphous magnetic fluid. Viscoelastic behaviours of magnetorheological fluids were established in rheological studies by Li *et al*. (2017) and Felicia and Philip (2014). More broadly, Melzner and Odenbach (2002) used the term "magnetoviscoelastic effect" to imply changes in elastic characteristics as well as viscosity changes caused by the application of an external magnetic field.

According to Felicia and Philip (2014), the connection and breaking of the (chain-like) side chains and the (drop-like) dense clusters are the essential mechanisms underlying the change in the dynamic viscoelastic behaviours of ferrofluids. The intermediate scattering function of the colloidal suspensions was shown to be in control of the temporal relaxation of the viscoelasticity and transport coefficient (Avdeev *et al*, 2002).

The Newtonian and Bingham plastic models have been widely utilized to describe the flow behaviour characteristics of magnetorheological fluids and was applied to the design of magnetorheological dampers. However, as the phenomenon of shear thinning or shear thickening exists in the flow of magnetorheological fluids, the Bingham-plastic may not be an accurate model to predict the behaviour of magnetorheological fluids. Therefore, Herschel-Bulkley model was also utilized to describe the flow properties of magnetorheological fluids. However, the viscosity associated with the Herschel-Buckley stress diverges to infinity as the strain rate approaches zero. This divergence makes the model difficult to implement in numerical simulations. A closer study of the behaviour of the fluid shows that the flow of magnetorheological fluids can be well modelled as viscoelastic fluids. Following the established elastic-viscous behaviours of magneto-rheological (MR) fluid and the viscoelastic properties of magnetorheological fluids, it is required that the flow characteristics of this fluid should be based on viscoelastic model. To be best of the authors' knowledge, such study has not been presented analytically. Therefore, in this work, the flow behaviour of magnetorheological fluid in valve and shear modes for damping system is modelled and analyzed analytically using Laplace transforms method. The influences of various parameters of the model on the velocity, pressure and shear stress distributions are studied.

2. Viscoelastic fluid Model for Magnetorheological Damper

The magnetorheological fluids flow between two parallel plates under the influence of magnetic field as shown in the Fig. 2. It is assumed that the flow of the fluid is laminar, stable, incompressible, isothermal, and non-reacting chemically. The fluid conducts electrical energy as it flows unsteadily under magnetic force field. The fluid structure is everywhere in thermodynamic equilibrium and the plate is maintained at constant temperature. Following the assumptions, the governing equations for the flow of the viscoelastic fluid are given as

$$\frac{\partial u}{\partial x} + \frac{\partial v}{\partial y} + \frac{\partial w}{\partial z} = 0 \tag{1}$$

$$\rho\left(\frac{\partial u}{\partial t} + u\frac{\partial u}{\partial x} + v\frac{\partial u}{\partial y} + w\frac{\partial u}{\partial z}\right) = \rho g_x - \frac{\partial p}{\partial x} + \beta_1\left(\frac{\partial^2 u}{\partial x^2} + \frac{\partial^2 u}{\partial y^2} + \frac{\partial^2 u}{\partial z^2}\right) + \beta_2\frac{\partial}{\partial t}\left(\frac{\partial^2 u}{\partial x^2} + \frac{\partial^2 u}{\partial y^2} + \frac{\partial^2 u}{\partial z^2}\right) - \sigma B_o^2 u - \frac{\mu_{nf} u}{K_p} \tag{2}$$

$$\rho\left(\frac{\partial v}{\partial t} + u\frac{\partial v}{\partial x} + v\frac{\partial v}{\partial y} + w\frac{\partial v}{\partial z}\right) = \rho g_y - \frac{\partial p}{\partial y} + \beta_1\left(\frac{\partial^2 v}{\partial x^2} + \frac{\partial^2 v}{\partial y^2} + \frac{\partial^2 v}{\partial z^2}\right) + \beta_2\frac{\partial}{\partial t}\left(\frac{\partial^2 v}{\partial x^2} + \frac{\partial^2 v}{\partial y^2} + \frac{\partial^2 v}{\partial z^2}\right) - \sigma B_o^2 v - \frac{\mu_{nf} v}{K_p} \tag{3}$$

$$\rho\left(\frac{\partial w}{\partial t} + u\frac{\partial w}{\partial x} + v\frac{\partial w}{\partial y} + w\frac{\partial w}{\partial z}\right) = \rho g_z - \frac{\partial p}{\partial z} + \beta_1\left(\frac{\partial^2 w}{\partial x^2} + \frac{\partial^2 w}{\partial y^2} + \frac{\partial^2 w}{\partial z^2}\right) + \beta_2\frac{\partial}{\partial t}\left(\frac{\partial^2 w}{\partial x^2} + \frac{\partial^2 w}{\partial y^2} + \frac{\partial^2 w}{\partial z^2}\right) - \sigma B_o^2 w - \frac{\mu_{nf} w}{K_p} \tag{4}$$

The flow is taking as two-directional, then

$$w = 0, \quad \frac{\partial w}{\partial x} = \frac{\partial w}{\partial y} = \frac{\partial w}{\partial z} = 0, \quad \frac{\partial^2 w}{\partial x^2} = \frac{\partial^2 w}{\partial y^2} = \frac{\partial^2 w}{\partial z^2} = 0, \quad \frac{\partial p}{\partial z} = 0, \quad \rho g_z = 0, \quad \frac{\partial w}{\partial t} = 0$$

$$\frac{\partial u}{\partial z} = \frac{\partial v}{\partial z} = \frac{\partial w}{\partial z} = 0, \quad \frac{\partial^2 u}{\partial z^2} = \frac{\partial^2 v}{\partial z^2} = \frac{\partial^2 w}{\partial z^2} = 0, \tag{5}$$

The wall is impermeable that the fluid cannot pass through the wall. So, the fluid cannot flow in the y-direction, then

$$v = 0, \quad \frac{\partial v}{\partial x} = \frac{\partial v}{\partial y} = \frac{\partial v}{\partial z} = 0, \quad \frac{\partial^2 v}{\partial x^2} = \frac{\partial^2 v}{\partial y^2} = \frac{\partial^2 v}{\partial z^2} = 0, \quad \frac{\partial v}{\partial t} = 0 \tag{6}$$

The gravity is only in y-direction so, gravity in the *x*-direction is eliminated, $\rho g_x = 0$

Therefore, the flow model equations reduce to

$$\frac{\partial u}{\partial x} = 0 \tag{7}$$

$$\rho \left(\frac{\partial u}{\partial t} + u \frac{\partial u}{\partial x} \right) = -\frac{\partial p}{\partial x} + \beta_1 \left(\frac{\partial^2 u}{\partial x^2} + \frac{\partial^2 u}{\partial y^2} \right) + \beta_2 \frac{\partial}{\partial t} \left(\frac{\partial^2 u}{\partial x^2} + \frac{\partial^2 u}{\partial y^2} \right) - \sigma B_o^2 u - \frac{\mu_{nf} u}{K_p} \tag{8}$$

$$0 = \rho g_y - \frac{\partial p}{\partial y} \tag{9}$$

The flow is fully developed i.e., the velocity in the direction of flow does not change

$$\frac{\partial u}{\partial x} = 0, \quad \frac{\partial^2 u}{\partial x^2} = 0 \tag{10}$$

Then the flow models reduce to

$$\rho \frac{\partial u}{\partial t} = -\frac{\partial p}{\partial x} + \beta_1 \frac{\partial^2 u}{\partial y^2} + \beta_2 \frac{\partial}{\partial t} \left(\frac{\partial^2 u}{\partial y^2} \right) - \sigma B_o^2 u - \frac{\mu_{nf} u}{K_p} \tag{11}$$

$$0 = \rho g_y - \frac{\partial p}{\partial y} \tag{12}$$

The initial condition
$$t = 0, \quad u = u_0, \quad 0 \le y \le h$$

The boundary conditions for the pressure driven flow mode

$$t > 0, \quad y = 0, \quad u = 0, \quad 0 \le y \le h \tag{13a}$$
$$t > 0, \quad y = h, \quad u = 0, \quad 0 \le y \le h \tag{13b}$$

The boundary conditions for the direct shear mode

$$t > 0, \quad y = 0, \quad u = 0, \quad 0 \le y \le h \tag{14a}$$
$$t > 0, \quad y = h, \quad u = U, \quad 0 \le y \le h \tag{14b}$$

The pressure gradient in direction of flow is taken as constant. Applying Laplace transform method, we have

$$\rho s \bar{u} = -\frac{\partial p}{s \partial x} + \beta_1 \frac{\partial^2 \bar{u}}{\partial y^2} + \beta_2 \left(\frac{\partial^2 \bar{u}}{\partial y^2} \right) s - \sigma B_o^2 \bar{u} - \frac{\mu_{nf} \bar{u}}{K_p} \tag{15}$$

Arranging Eq. (15)

$$\left(\beta_2 s + \beta_1 \right) \frac{\partial^2 \bar{u}}{\partial y^2} - \left(\rho s + \sigma B_o^2 + \frac{\mu_{nf}}{K_p} \right) \bar{u} = \frac{\partial p}{s \partial x} \tag{16}$$

On solving Eq. (16), we have

$$\bar{u} = A \cos \left(\sqrt{\frac{\rho s + \sigma B_o^2 + \frac{\mu_{nf}}{K_p}}{\left(\beta_2 s + \beta_1 \right)}} \, y \right) + B \sin \left(\sqrt{\frac{\rho s + \sigma B_o^2 + \frac{\mu_{nf}}{K_p}}{\left(\beta_2 s + \beta_1 \right)}} \, y \right) + \frac{\left(\frac{\partial p}{\partial x} \right)}{s \left(\beta_2 s + \beta_1 \right) \left(\rho s + \sigma B_o^2 + \frac{\mu_{nf}}{K_p} \right)} \tag{17}$$

The boundary conditions in Laplace transform domain for the pressure driven flow mode

$$s > 0, \ y = 0, \ \bar{u} = 0, \ 0 \le y \le h \tag{18a}$$
$$s > 0, \ y = h, \ \bar{u} = 0, \ 0 \le y \le h \tag{18b}$$

The boundary conditions in Laplace transform domain for the direct shear mode

$$s > 0, \ y = 0, \ \bar{u} = 0, \ 0 \le y \le h \tag{19a}$$
$$s > 0, \ y = h, \ \bar{u} = \frac{U}{s}, \ 0 \le y \le h \tag{19b}$$

Applying the boundary conditions to Eq. (17), we have **for the pressure driven flow mode**

$$A = \frac{-\left(\frac{\partial p}{\partial x} \right)}{s \left(\beta_2 s + \beta_1 \right) \left(\rho s + \sigma B_o^2 + \frac{\mu_{nf}}{K_p} \right)}$$

$$B = \frac{\dfrac{\left(\frac{\partial p}{\partial x} \right)}{s \left(\beta_2 s + \beta_1 \right) \left(\rho s + \sigma B_o^2 + \frac{\mu_{nf}}{K_p} \right)} \cos \left(\sqrt{\frac{\rho s + \sigma B_o^2 + \frac{\mu_{nf}}{K_p}}{\left(\beta_2 s + \beta_1 \right)}} \, h \right) - \dfrac{\left(\frac{\partial p}{\partial x} \right)}{s \left(\beta_2 s + \beta_1 \right) \left(\rho s + \sigma B_o^2 + \frac{\mu_{nf}}{K_p} \right)}}{\sin \left(\sqrt{\frac{\rho s + \sigma B_o^2 + \frac{\mu_{nf}}{K_p}}{\left(\beta_2 s + \beta_1 \right)}} \, h \right)}$$

Therefore, we have

$$\bar{u} = \frac{1}{sin\left(\sqrt{\frac{\rho s+\sigma B_o^2+\frac{\mu_{nf}}{K_p}}{(\beta_2 s+\beta_1)}}\,h\right)}\left\{\left[\frac{\left(\frac{\partial p}{\partial x}\right)}{s(\beta_2 s+\beta_1)\left(\rho s+\sigma B_o^2+\frac{\mu_{nf}}{K_p}\right)}\left[\begin{matrix}cos\left(\sqrt{\frac{\rho s+\sigma B_o^2+\frac{\mu_{nf}}{K_p}}{(\beta_2 s+\beta_1)}}\right)hsin\left(\sqrt{\frac{\rho s+\sigma B_o^2+\frac{\mu_{nf}}{K_p}}{(\beta_2 s+\beta_1)}}\,y\right)\\ -sin\left(\sqrt{\frac{\rho s+\sigma B_o^2+\frac{\mu_{nf}}{K_p}}{(\beta_2 s+\beta_1)}}\right)hcos\left(\sqrt{\frac{\rho s+\sigma B_o^2+\frac{\mu_{nf}}{K_p}}{(\beta_2 s+\beta_1)}}\,y\right)\end{matrix}\right]\right] \\ \left[-\frac{\left(\frac{\partial p}{\partial x}\right)sin\left(\sqrt{\frac{\rho s+\sigma B_o^2+\frac{\mu_{nf}}{K_p}}{(\beta_2 s+\beta_1)}}\,y\right)}{s(\beta_2 s+\beta_1)\left(\rho s+\sigma B_o^2+\frac{\mu_{nf}}{K_p}\right)}+\frac{\left(\frac{\partial p}{\partial x}\right)sin\left(\sqrt{\frac{\rho s+\sigma B_o^2+\frac{\mu_{nf}}{K_p}}{(\beta_2 s+\beta_1)}}\,h\right)}{s(\beta_2 s+\beta_1)\left(\rho s+\sigma B_o^2+\frac{\mu_{nf}}{K_p}\right)}\right]\right\} \tag{20}$$

Which can be written as

$$\bar{u}(y,s) = \frac{\left(\frac{\partial p}{\partial x}\right)}{s(\beta_2 s+\beta_1)\left(\rho s+\sigma B_o^2+\frac{\mu_{nf}}{K_p}\right)}\frac{sin\left(\sqrt{\frac{\rho s+\sigma B_o^2+\frac{\mu_{nf}}{K_p}}{(\beta_2 s+\beta_1)}}(h-y)\right)}{sin\left(\sqrt{\frac{\rho s+\sigma B_o^2+\frac{\mu_{nf}}{K_p}}{(\beta_2 s+\beta_1)}}\,h\right)}-\frac{\left(\frac{\partial p}{\partial x}\right)sin\left(\sqrt{\frac{\rho s+\sigma B_o^2+\frac{\mu_{nf}}{K_p}}{(\beta_2 s+\beta_1)}}\,y\right)}{s(\beta_2 s+\beta_1)\left(\rho s+\sigma B_o^2+\frac{\mu_{nf}}{K_p}\right)sin\left(\sqrt{\frac{\rho s+\sigma B_o^2+\frac{\mu_{nf}}{K_p}}{(\beta_2 s+\beta_1)}}\,h\right)}+\frac{\left(\frac{\partial p}{\partial x}\right)}{s(\beta_2 s+\beta_1)\left(\rho s+\sigma B_o^2+\frac{\mu_{nf}}{K_p}\right)} \tag{21}$$

For the direct shear mode

$$A = \frac{-\left(\frac{\partial p}{\partial x}\right)}{s(\beta_2 s+\beta_1)\left(\rho s+\sigma B_o^2+\frac{\mu_{nf}}{K_p}\right)}$$

$$B = \frac{U}{s\,sin\left(\sqrt{\frac{\rho s+\sigma B_o^2+\frac{\mu_{nf}}{K_p}}{(\beta_2 s+\beta_1)}}\,h\right)}+\frac{\left(\frac{\partial p}{\partial x}\right)cos\left(\sqrt{\frac{\rho s+\sigma B_o^2+\frac{\mu_{nf}}{K_p}}{(\beta_2 s+\beta_1)}}\,h\right)}{s(\beta_2 s+\beta_1)\left(\rho s+\sigma B_o^2+\frac{\mu_{nf}}{K_p}\right)sin\left(\sqrt{\frac{\rho s+\sigma B_o^2+\frac{\mu_{nf}}{K_p}}{(\beta_2 s+\beta_1)}}\,h\right)}$$

$$-\frac{\left(\frac{\partial p}{\partial x}\right)}{s(\beta_2 s+\beta_1)\left(\rho s+\sigma B_o^2+\frac{\mu_{nf}}{K_p}\right)sin\left(\sqrt{\frac{\rho s+\sigma B_o^2+\frac{\mu_{nf}}{K_p}}{(\beta_2 s+\beta_1)}}\,h\right)}$$

Then, we have

$$\bar{u}(y,s) = \frac{\left(\frac{\partial p}{\partial x}\right)}{s(\beta_2 s + \beta_1)\left(\rho s + \sigma B_o^2 + \frac{\mu_{nf}}{K_p}\right)} \frac{\sin\left(\sqrt{\frac{\rho s + \sigma B_o^2 + \frac{\mu_{nf}}{K_p}}{(\beta_2 s + \beta_1)}}(h-y)\right)}{\sin\left(\sqrt{\frac{\rho s + \sigma B_o^2 + \frac{\mu_{nf}}{K_p}}{(\beta_2 s + \beta_1)}}h\right)} - \frac{\left(\frac{\partial p}{\partial x}\right)\sin\left(\sqrt{\frac{\rho s + \sigma B_o^2 + \frac{\mu_{nf}}{K_p}}{(\beta_2 s + \beta_1)}}y\right)}{s(\beta_2 s + \beta_1)\left(\rho s + \sigma B_o^2 + \frac{\mu_{nf}}{K_p}\right)\sin\left(\sqrt{\frac{\rho s + \sigma B_o^2 + \frac{\mu_{nf}}{K_p}}{(\beta_2 s + \beta_1)}}h\right)}$$

$$+ \frac{\left(\frac{\partial p}{\partial x}\right)}{s(\beta_2 s + \beta_1)\left(\rho s + \sigma B_o^2 + \frac{\mu_{nf}}{K_p}\right)} + \frac{U\sin\left(\sqrt{\frac{\rho s + \sigma B_o^2 + \frac{\mu_{nf}}{K_p}}{(\beta_2 s + \beta_1)}}y\right)}{s\,\sin\left(\sqrt{\frac{\rho s + \sigma B_o^2 + \frac{\mu_{nf}}{K_p}}{(\beta_2 s + \beta_1)}}h\right)}$$

(22)

Due to the complexity in finding the inverse Laplace transforms of Eqs. (21) and (22), a numerical evaluation of the inverse Laplace transform is carried out using Simon's approach [4] given as

$$u(y,t) = \frac{e^{a_p t}}{t}\left[\frac{1}{2}\bar{u}(y,a_p) + \sum_{n=1}^{N} Re\left[\bar{u}\left(y,a_p + i\frac{n\pi}{a_p}\right)\right](-1)^n\right]$$

(23)

Where **for the pressure driven flow mode**

$$\bar{u}(y,a_p) = \frac{\left(\frac{\partial p}{\partial x}\right)}{a_p(\beta_2 s + \beta_1)\left(\rho a_p + \sigma B_o^2 + \frac{\mu_{nf}}{K_p}\right)} \frac{\sin\left(\sqrt{\frac{\rho a_p + \sigma B_o^2 + \frac{\mu_{nf}}{K_p}}{(\beta_2 a_p + \beta_1)}}(h-y)\right)}{\sin\left(\sqrt{\frac{\rho a_p + \sigma B_o^2 + \frac{\mu_{nf}}{K_p}}{(\beta_2 a_p + \beta_1)}}h\right)} - \frac{\left(\frac{\partial p}{\partial x}\right)\sin\left(\sqrt{\frac{\rho a_p + \sigma B_o^2 + \frac{\mu_{nf}}{K_p}}{(\beta_2 a_p + \beta_1)}}y\right)}{a_p(\beta_2 a_p + \beta_1)\left(\rho a_p + \sigma B_o^2 + \frac{\mu_{nf}}{K_p}\right)\sin\left(\sqrt{\frac{\rho a_p + \sigma B_o^2 + \frac{\mu_{nf}}{K_p}}{(\beta_2 a_p + \beta_1)}}h\right)} + \frac{\left(\frac{\partial p}{\partial x}\right)}{a_p(\beta_2 a_p + \beta_1)\left(\rho a_p + \sigma B_o^2 + \frac{\mu_{nf}}{K_p}\right)}$$

$$\bar{u}\left(y,a_p + i\frac{n\pi}{a_p}\right) = \frac{\left(\frac{\partial p}{\partial x}\right)}{\left(a_p + i\frac{n\pi}{a_p}\right)\left(\beta_2\left(a_p + i\frac{n\pi}{a_p}\right) + \beta_1\right)\left(\rho\left(a_p + i\frac{n\pi}{a_p}\right) + \sigma B_o^2 + \frac{\mu_{nf}}{K_p}\right)} \frac{\sin\left(\sqrt{\frac{\rho\left(a_p + i\frac{n\pi}{a_p}\right) + \sigma B_o^2 + \frac{\mu_{nf}}{K_p}}{\left(\beta_2\left(a_p + i\frac{n\pi}{a_p}\right) + \beta_1\right)}}(h-y)\right)}{\sin\left(\sqrt{\frac{\rho\left(a_p + i\frac{n\pi}{a_p}\right) + \sigma B_o^2 + \frac{\mu_{nf}}{K_p}}{\left(\beta_2\left(a_p + i\frac{n\pi}{a_p}\right) + \beta_1\right)}}h\right)}$$

$$- \frac{\left(\frac{\partial p}{\partial x}\right)\sin\left(\sqrt{\frac{\rho s + \sigma B_o^2 + \frac{\mu_{nf}}{K_p}}{(\beta_2 s + \beta_1)}}y\right)}{s(\beta_2 s + \beta_1)\left(\rho s + \sigma B_o^2 + \frac{\mu_{nf}}{K_p}\right)\sin\left(\sqrt{\frac{\rho s + \sigma B_o^2 + \frac{\mu_{nf}}{K_p}}{(\beta_2 s + \beta_1)}}h\right)} + \frac{\left(\frac{\partial p}{\partial x}\right)}{s(\beta_2 s + \beta_1)\left(\rho s + \sigma B_o^2 + \frac{\mu_{nf}}{K_p}\right)}$$

For the direct mode

$$\bar{u}(y,a_p) = \frac{\left(\frac{\partial p}{\partial x}\right)}{a_p\left(\beta_2 a_p + \beta_1\right)\left(\rho a_p + \sigma B_o^2 + \frac{\mu_{nf}}{K_p}\right)} \frac{sin\left(\sqrt{\frac{\rho a_p + \sigma B_o^2 + \frac{\mu_{nf}}{K_p}}{(\beta_2 a_p + \beta_1)}}(h-y)\right)}{sin\left(\sqrt{\frac{\rho a_p + \sigma B_o^2 + \frac{\mu_{nf}}{K_p}}{(\beta_2 a_p + \beta_1)}}h\right)} - \frac{\left(\frac{\partial p}{\partial x}\right)sin\left(\sqrt{\frac{\rho a_p + \sigma B_o^2 + \frac{\mu_{nf}}{K_p}}{(\beta_2 a_p + \beta_1)}}y\right)}{a_p\left(\beta_2 a_p + \beta_1\right)\left(\rho a_p + \sigma B_o^2 + \frac{\mu_{nf}}{K_p}\right)sin\left(\sqrt{\frac{\rho a_p + \sigma B_o^2 + \frac{\mu_{nf}}{K_p}}{(\beta_2 a_p + \beta_1)}}h\right)}$$

$$+ \frac{\left(\frac{\partial p}{\partial x}\right)}{a_p\left(\beta_2 a_p + \beta_1\right)\left(\rho a_p + \sigma B_o^2 + \frac{\mu_{nf}}{K_p}\right)} + \frac{Usin\left(\sqrt{\frac{\rho a_p + \sigma B_o^2 + \frac{\mu_{nf}}{K_p}}{(\beta_2 a_p + \beta_1)}}y\right)}{s\ sin\left(\sqrt{\frac{\rho a_p + \sigma B_o^2 + \frac{\mu_{nf}}{K_p}}{(\beta_2 a_p + \beta_1)}}h\right)}$$

$$\bar{u}\left(y,a_p + i\frac{n\pi}{a_p}\right) = \frac{\left(\frac{\partial p}{\partial x}\right)}{\left(a_p + i\frac{n\pi}{a_p}\right)\left(\beta_2\left(a_p + i\frac{n\pi}{a_p}\right) + \beta_1\right)\left(\rho\left(a_p + i\frac{n\pi}{a_p}\right) + \sigma B_o^2 + \frac{\mu_{nf}}{K_p}\right)} \frac{sin\left(\sqrt{\frac{\rho\left(a_p + i\frac{n\pi}{a_p}\right) + \sigma B_o^2 + \frac{\mu_{nf}}{K_p}}{\left(\beta_2\left(a_p + i\frac{n\pi}{a_p}\right) + \beta_1\right)}}(h-y)\right)}{sin\left(\sqrt{\frac{\rho\left(a_p + i\frac{n\pi}{a_p}\right) + \sigma B_o^2 + \frac{\mu_{nf}}{K_p}}{\left(\beta_2\left(a_p + i\frac{n\pi}{a_p}\right) + \beta_1\right)}}h\right)}$$

$$- \frac{\left(\frac{\partial p}{\partial x}\right)sin\left(\sqrt{\frac{\rho\left(a_p + i\frac{n\pi}{a_p}\right) + \sigma B_o^2 + \frac{\mu_{nf}}{K_p}}{\left(\beta_2\left(a_p + i\frac{n\pi}{a_p}\right) + \beta_1\right)}}y\right)}{\left(a_p + i\frac{n\pi}{a_p}\right)\left(\beta_2\left(a_p + i\frac{n\pi}{a_p}\right) + \beta_1\right)\left(\rho\left(a_p + i\frac{n\pi}{a_p}\right) + \sigma B_o^2 + \frac{\mu_{nf}}{K_p}\right)sin\left(\sqrt{\frac{\rho\left(a_p + i\frac{n\pi}{a_p}\right) + \sigma B_o^2 + \frac{\mu_{nf}}{K_p}}{\left(\beta_2\left(a_p + i\frac{n\pi}{a_p}\right) + \beta_1\right)}}h\right)}$$

$$+ \frac{\left(\frac{\partial p}{\partial x}\right)}{\left(a_p + i\frac{n\pi}{a_p}\right)\left(\beta_2\left(\left(a_p + i\frac{n\pi}{a_p}\right) + i\frac{n\pi}{a_p}\right) + \beta_1\right)\left(\rho\left(a_p + i\frac{n\pi}{a_p}\right) + \sigma B_o^2 + \frac{\mu_{nf}}{K_p}\right)} + \frac{Usin\left(\sqrt{\frac{\rho\left(\left(a_p + i\frac{n\pi}{a_p}\right) + i\frac{n\pi}{a_p}\right) + \sigma B_o^2 + \frac{\mu_{nf}}{K_p}}{\left(\beta_2\left(\left(a_p + i\frac{n\pi}{a_p}\right) + i\frac{n\pi}{a_p}\right) + \beta_1\right)}}y\right)}{s\ sin\left(\sqrt{\frac{\rho\left(a_p + i\frac{n\pi}{a_p}\right) + \sigma B_o^2 + \frac{\mu_{nf}}{K_p}}{\left(\beta_2\left(a_p + i\frac{n\pi}{a_p}\right) + \beta_1\right)}}h\right)}$$

It was suggested by Lee *et al*. [5] that the values of $a_p t$ in Eqs. (21) and (22) range between 4 and 5. Because of absence of oscillating cosine and sine functions, Eqs. (22) and (23) converges more quickly because. The optimally value of $a_p t$ is 4.7 [5]

Analysis of Shear Stress, Pressure Drop and Mass Flow Rate of the fluid

The shear stresses at the lower and upper plates are given as

$$\tau_0 = \mu \frac{\partial u}{\partial y}\bigg|_{y=0} \tag{24}$$

$$\tau_h = \mu \frac{\partial u}{\partial y}\bigg|_{y=h} \tag{25}$$

The volume flow rate per unit width at normal section of the channel is given by

$$Q = \int_0^L u(y,t)dy \tag{26}$$

The pressure loss due to viscous drag at normal section of the channel is given by

$$\int_L^0 dp = -\int_L^0 \frac{12\mu u(y,t)}{h^2} dy \tag{27}$$

Which is given as

$$p_0 - p_L = -\frac{12\mu}{h^2} \int_L^0 u(y,t)dy \tag{28}$$

Substituting Eq. (26) into Eq. (28), we arrived at viscous pressure loss as

$$p_0 - p_L = \frac{12\mu Q}{h^2} \tag{29}$$

There are two independent sets of equations used to determine the magnetorheological damper force in the different modes. Pressure driven flow mode has two components to the pressure drop: pressure loss due to viscous drag which is given in Eq. (27), and pressure loss due to the field dependent yield stress. On the other hand, the pressure drop due to the increment of the yield stress of the MR fluid. The magnetic field-dependent yield stress pressure loss is given as

$$p_{MR} = \frac{2cL_p\tau_y(B)}{h} \tag{30}$$

Where c is a coefficient that depends on flow velocity profile and has a value range from 2.0 to 3.0, L_p is the length of the magnetic pole, h is the distance between the upper and lower plates, and $\tau_y(B)$ is the yield stress caused by the magnetic flux density B. Therefore, t_g is the magnetic field dependent-yield stress.

Therefore, the total pressure loss is given as

$$\Delta p_{total} = \frac{12\mu Q}{h^2} + \frac{2cL_p\tau_y(B)}{h} \tag{31}$$

Alternatively, one can write

$$\Delta p_{total} = \frac{12\mu QL}{\lambda^3 w} + \frac{cL_p\tau_y}{\lambda} \tag{32}$$

μ is the fluid viscosity, Q is the flowrate, L is the plate length, w is the pole width, λ is the fluid gap, and t_g is the field dependent yield stress.

The damper force is given by

$$F = \frac{\mu u_r A}{\lambda} + \tau_y A \tag{33}$$

Where
u_r is the relative velocity between the plates and A is the pole area.

For the steady state model, we have

$$+\frac{\partial^2 u}{\partial y^2} - \frac{1}{\beta_1}\left(\sigma B_o^2 + \frac{\mu_{nf}}{K_p}\right)u = \frac{1}{\beta_1}\frac{\partial p}{\partial x}$$

Using the boundary conditions, for the valve mode, we arrived at

$$u(y) = \frac{\frac{\partial p}{\partial x}}{\left(\sigma B_o^2 + \frac{\mu_{nf}}{K_p}\right)}\left[\left\{\frac{sinh\sqrt{\left(\sigma B_o^2 + \frac{\mu_{nf}}{K_p}\right)}(h-y)}{sinh\sqrt{\left(\sigma B_o^2 + \frac{\mu_{nf}}{K_p}\right)}h} + \frac{sinh\sqrt{\left(\sigma B_o^2 + \frac{\mu_{nf}}{K_p}\right)}y}{sinh\sqrt{\left(\sigma B_o^2 + \frac{\mu_{nf}}{K_p}\right)}h}\right\} - 1\right]$$

For the direct shear mode

$$u(y) = \left[\frac{\frac{\partial p}{\partial x}}{\left(\sigma B_o^2 + \frac{\mu_{nf}}{K_p}\right)}\left\{\frac{sinh\sqrt{\left(\sigma B_o^2 + \frac{\mu_{nf}}{K_p}\right)}(h-y)}{sinh\sqrt{\left(\sigma B_o^2 + \frac{\mu_{nf}}{K_p}\right)}h} + \frac{sinh\sqrt{\left(\sigma B_o^2 + \frac{\mu_{nf}}{K_p}\right)}y}{sinh\sqrt{\left(\sigma B_o^2 + \frac{\mu_{nf}}{K_p}\right)}h}\right\} - 1\right] + \frac{Usinh\sqrt{\left(\sigma B_o^2 + \frac{\mu_{nf}}{K_p}\right)}y}{sinh\sqrt{\left(\sigma B_o^2 + \frac{\mu_{nf}}{K_p}\right)}h}$$

Analysis of Shear Stress, Pressure Drop and Mass Flow Rate of the fluid

The shear stresses at the lower and upper plates in the valve mode are given as

$$\tau_0 = \mu\frac{\partial p}{\partial x}\left\{\frac{1-cosh\sqrt{\left(\sigma B_o^2 + \frac{\mu_{nf}}{K_p}\right)}h}{sinh\sqrt{\left(\sigma B_o^2 + \frac{\mu_{nf}}{K_p}\right)}h}\right\} \tag{24}$$

$$\tau_h = \mu\frac{\partial p}{\partial x}\left\{\frac{1+cosh\sqrt{\left(\sigma B_o^2 + \frac{\mu_{nf}}{K_p}\right)}h}{sinh\sqrt{\left(\sigma B_o^2 + \frac{\mu_{nf}}{K_p}\right)}h}\right\} \tag{25}$$

The shear stresses at the lower and upper plates in the direct shear mode are given as

$$\tau_0 = \mu \left[\frac{\partial p}{\partial x} \left\{ \frac{1 - \cosh\sqrt{\left(\sigma B_o^2 + \frac{\mu_{nf}}{K_p}\right)}h}{\sinh\sqrt{\left(\sigma B_o^2 + \frac{\mu_{nf}}{K_p}\right)}h} \right\} + \frac{U\sqrt{\left(\sigma B_o^2 + \frac{\mu_{nf}}{K_p}\right)}\cosh\sqrt{\left(\sigma B_o^2 + \frac{\mu_{nf}}{K_p}\right)}h}{\sinh\sqrt{\left(\sigma B_o^2 + \frac{\mu_{nf}}{K_p}\right)}h} \right] \quad (24)$$

$$\tau_h = \mu \left[\frac{\partial p}{\partial x} \left\{ \frac{1 + \cosh\sqrt{\left(\sigma B_o^2 + \frac{\mu_{nf}}{K_p}\right)}h}{\sinh\sqrt{\left(\sigma B_o^2 + \frac{\mu_{nf}}{K_p}\right)}h} \right\} + \frac{U\sqrt{\left(\sigma B_o^2 + \frac{\mu_{nf}}{K_p}\right)}\cosh\sqrt{\left(\sigma B_o^2 + \frac{\mu_{nf}}{K_p}\right)}h}{\sinh\sqrt{\left(\sigma B_o^2 + \frac{\mu_{nf}}{K_p}\right)}h} \right] \quad (25)$$

The volume flow rate per unit width at normal section of the channel is given by

$$Q = \int_0^L u(y,t)dy \quad (26)$$

The pressure loss due to viscous drag at normal section of the channel is given by

$$\int_L^0 dp = -\int_L^0 \frac{12\mu u(y,t)}{h^2} dy \quad (27)$$

Which is given as

$$p_0 - p_L = -\frac{12\mu}{h^2}\int_L^0 u(y,t)dy \quad (28)$$

Substituting Eq. (26) into Eq. (28), we arrived at viscous pressure loss as

$$p_0 - p_L = \frac{12\mu Q}{h^2} \quad (29)$$

There are two independent sets of equations used to determine the magnetorheological damper force in the different modes. Pressure driven flow mode has two components to the pressure drop: pressure loss due to viscous drag which is given in Eq. (27), and pressure loss due to the field dependent yield stress. On the other hand, the pressure drop due to the increment of the yield stress of the MR fluid. The magnetic field-dependent yield stress pressure loss is given as

$$p_{MR} = \frac{2cL_p\tau_y(B)}{h} \quad (30)$$

Where c is a coefficient that depends on flow velocity profile and has a value range from 2.0 to 3.0, L_p is the length of the magnetic pole, h is the distance between the upper and lower plates, and $\tau_y(B)$ is the yield stress caused by the magnetic flux density B. Therefore, t_g is the magnetic field dependent-yield stress. Therefore, the total pressure loss is given as

$$\Delta p_{total} = \frac{12\mu Q}{h^2} + \frac{2cL_p\tau_y(B)}{h} \quad (31)$$

Alternatively, one can write

$$\Delta p_{total} = \frac{12\mu QL}{\lambda^3 w} + \frac{cL_p \tau_y}{\lambda} \qquad (32)$$

μ is the fluid viscosity, Q is the flowrate, L is the plate length, w is the pole width, λ is the fluid gap, and t_g is the field dependent yield stress.

The damper force is given by

$$F = \frac{\mu u_r A}{\lambda} + \tau_y A \qquad (33)$$

4. Results and Discussion

The developed model solutions were simulated in MATLAB R2024a for the graphical visualizations of the flow behaviour of the MRF and for the studies of the significances of various parameters on the flow response of the MRF. The nonlinear flow behavior of magnetorheological fluid is demonstrated in the Fig. 3.
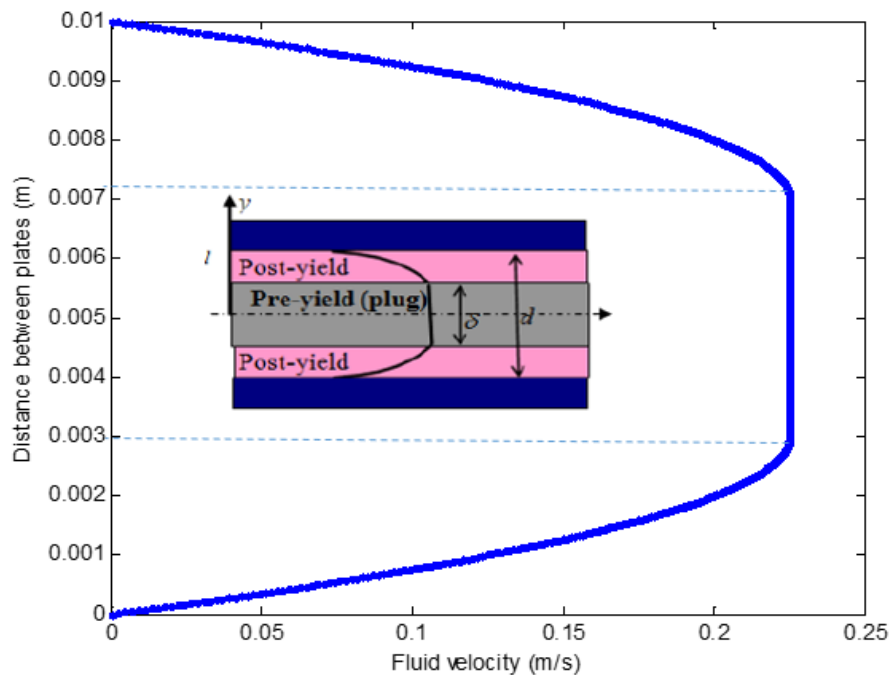
Figure 3. Viscoelastic flow model description of the magnetorheological fluid. When the magnetic field strength is (a) 100 kA/m (b) 400 kA/m

The model simulation shown in the figure as previously stated that the rheological behaviour of the fluid is separated into distinct pre-yield and post-yield regimes. The velocity profile is divided into three regions where the region in the middle represents the plug/pre-yield region in which the shear stress is zero. However, other regions contain post-yield where shear stress distributions are linear. The maximum and the minimum shear stresses are observed on the inner surfaces of the upper and lower plates. This result establishes that the viscoelastic model provides good description of the fluid flow model as predicted in experimental studies as well as theoretical studies using Bingham plastic model and the Herschel–Bulkley plastic models. With the aid of Bingham plastic model and the Herschel–Bulkley plastic models, the past studies had shown that the phenomenon of shear thinning or shear thickening exists in the flow of magnetorheological fluids. The present

work which adopts viscoelastic fluid flow model, also accounts for the post-yield shear thinning or thickening behaviour of magnetorheological fluids as depicted in Fig. 3.

Figs. 4-7 show the effect of pressure drop and magnetic field intensity on the MRF velocity distribution between the parallel plates. The figure shows pressure-driven/valve flow mode where the magnetorheological fluid is in between two fixed magnetic plates which produces magnetic flux. When the magnetic field is applied, magnetorheological particles align parallel to the applied magnetic field lines and resist the flow of the pressurized magnetorheological fluid. It is shown that an increase in the pressure drop enhances the fluid flow velocity.

Also, as the magnetic field intensity increases, the resistance to flow by the magnetorheological fluid increases. Consequently, the flow velocity of the fluid increases. This shows that the flow and rheological characteristics of the fluid changes when magnetic field is applied. In fact, the intensity of applied magnetic field is used to control the viscosity of the fluid. Such an excellent characteristics and special behavior of magnetorheological fluid has led to its vast of applications such as dampers, shock absorbers, rotary brakes, prosthetic devices, clutches, polishing and grinding devices, etc. It should be re-emphasized that the magnetic permeability is proportional to the volume fraction of particles. It is therefore reasonable to suppose that as the flux density increases, the tendency of the magnetic particles to align themselves along the lines of magnetic flux and create more resistance to the carrier fluid movement will increase. This obviously depict that as the volume fraction of particles increased, the fluid viscosity increases, in consequent, the resistance of the fluid to flow will increase.

Therefore, higher forces will be needed to cause the MRF to flow as the volume fraction increases. The post-yield region exhibited a highly steep slope in the stress-strain relationship. Because the volume fraction of particles was expected to increase more quickly under these conditions, the mechanisms also helped to explain why the slope was much steeper when the magnetic field intensity was high.
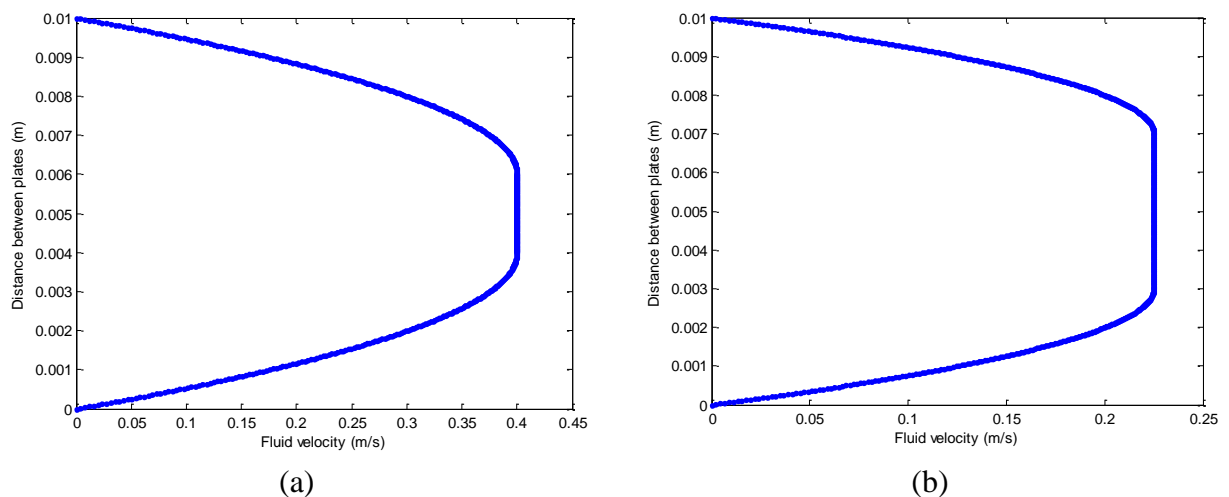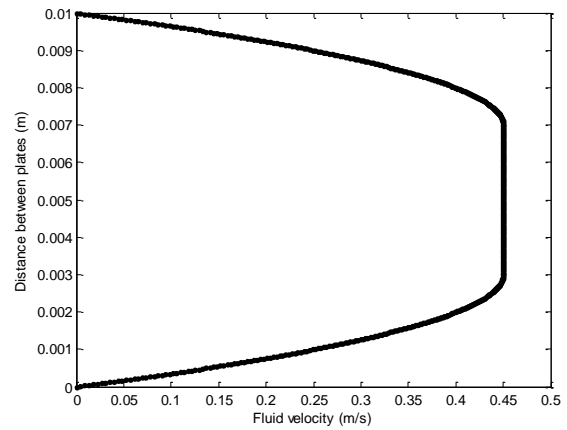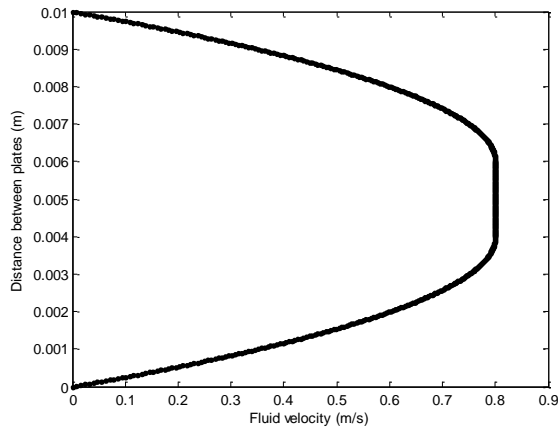

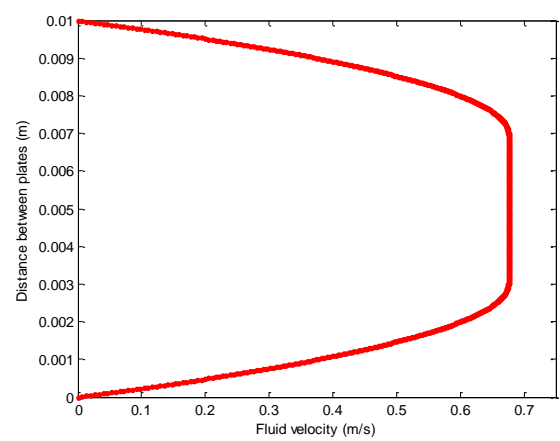(a)   (b)
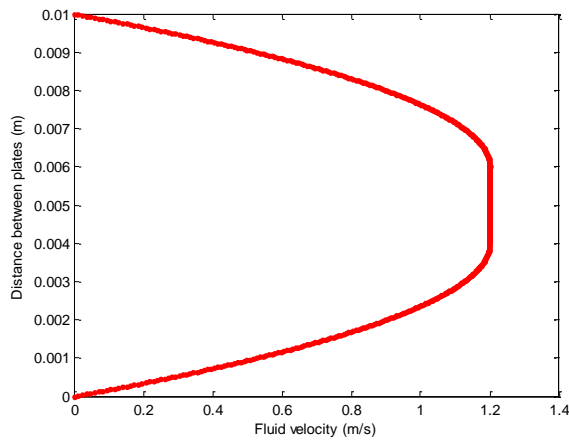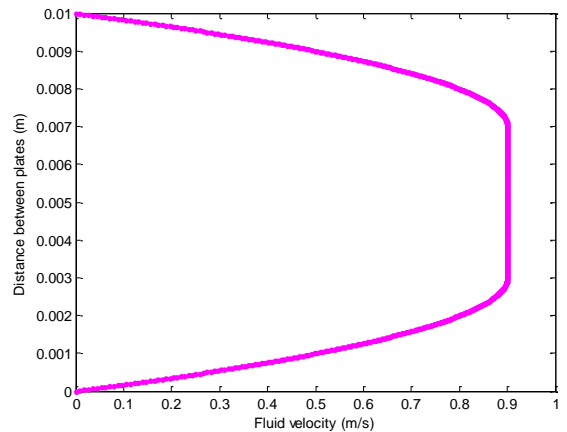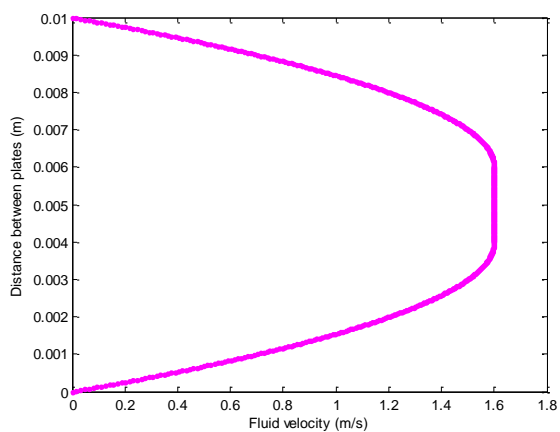
Figure 4 Effect of pre-yield and post-yield on the velocity distribution in the parallel plates of shock absorber when the pressure drop is 0.25 N/m^2

(a)

(b)

Figure 5 Effect of pre-yield and post-yield on the velocity distribution in the parallel plates of shock absorber when the pressure drop is 0.50 N/m². When the magnetic field strength is (a) 100 kA/m (b) 400 kA/m

(a)

(b)

Figure 6 Effect of pre-yield and post-yield on the velocity distribution in the parallel plates of shock absorber when the pressure drop is 0.75 N/m². When the magnetic field strength is (a) 100 kA/m (b) 400 kA/m

(a)

(b)

Figure 7 Effect of pre-yield and post-yield on the velocity distribution in the parallel plates of shock absorber when the pressure drop is 1.0 N/m². When the magnetic field strength is (a) 100 kA/m (b) 400 kA/m
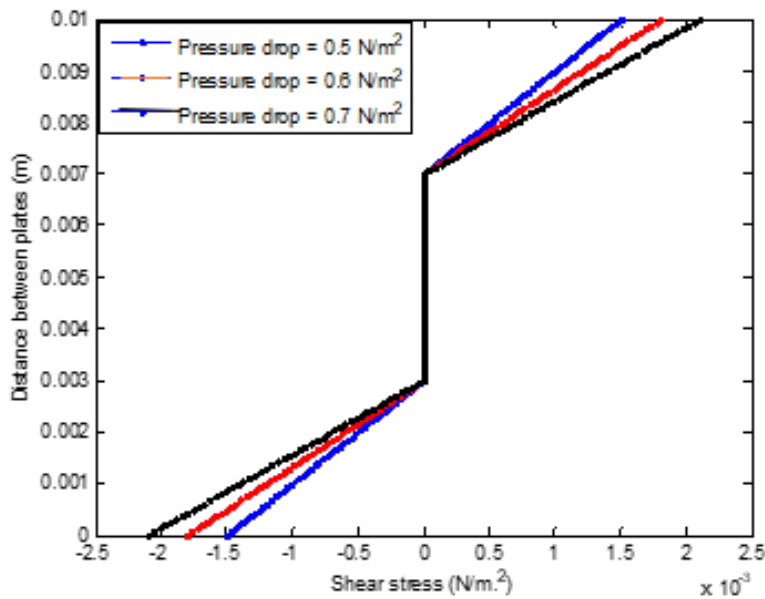
Figure 8 Effect of pressure drop on the shear stress distribution in the parallel horizontal plates of the shock absorber

It should be not that particle agglomeration may occur for high values of volume fractions that are close to the maximum packing density of the solid particles. As a result, some of the carrier fluid is trapped, which lowers the effective volume needed for the "free" carrier fluid to circulate. If this happened, the flow would encounter more resistance, and higher compressive stresses would be required to overcome this resistance.

Fig. 8 shows the shear stress distribution between the parallel plates. The figure shows that there are three sections in the velocity profile; the plug/pre-yield zone, where the shear stress is zero, is represented by the middle region. Shear stress distributions in other locations, on the other hand, are linear due to post-yield. The inner surfaces of the upper and lower plates exhibit the maximum and least shear stresses, respectively. Also, the figure presents the impact of pressure drop on the shear stress distribution between the plates. When shear stress increases as the pressure drop is augmented. This is because an increased pressure drop causes increase in the flow velocity as well as the velocity gradient, which in consequently increases the shear stress of the fluid.

Fig. 9 illustrates the significance of carrier (base fluid) and the magnetic field strength on yield stress of the magnetorheological fluid. In the figure, it is depicted that silicon oil, hydrocarbon oil and water as the carriers in the damper. It is shown that when the magnetic field strength is increased, the yield stress of the fluid also increases. In the base fluid applied, silicon displays the highest yield stress while water produces the lowest value of yield stress. Such a response is due to the viscosities, where silicon has the highest viscosity and water has the lowest.

Fig. 10 and 11 show the validation of the present work with the experiment performed by the authors. The results of the model show an excellent agreement with the experimental results. Therefore, the present model will support the design of dampers, shock absorbers, rotary brakes, prosthetic devices, clutches, polishing and grinding devices, etc.
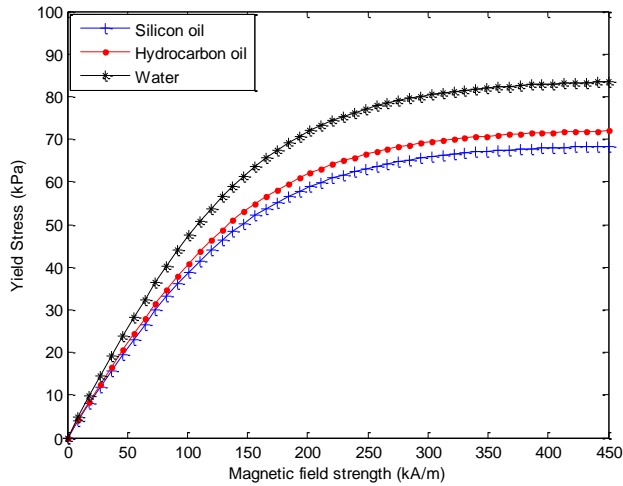
Figure 9 Effect of carrier fluid and magnetic field strength on the yield stress in the parallel horizontal plates
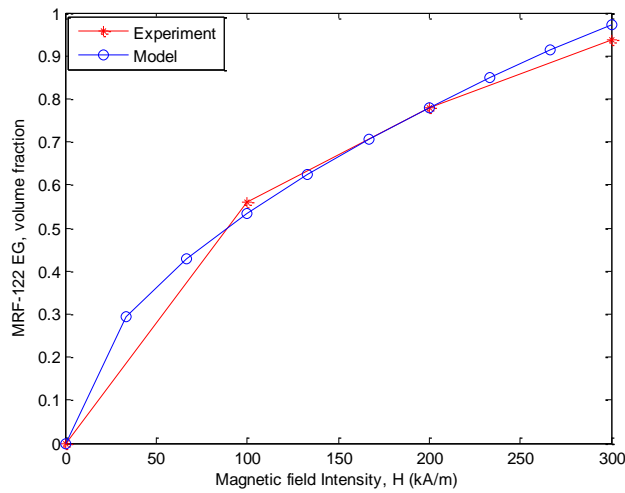

Figure 10. Experimental validation of the model results of volume fraction of MRF against magnetic strength
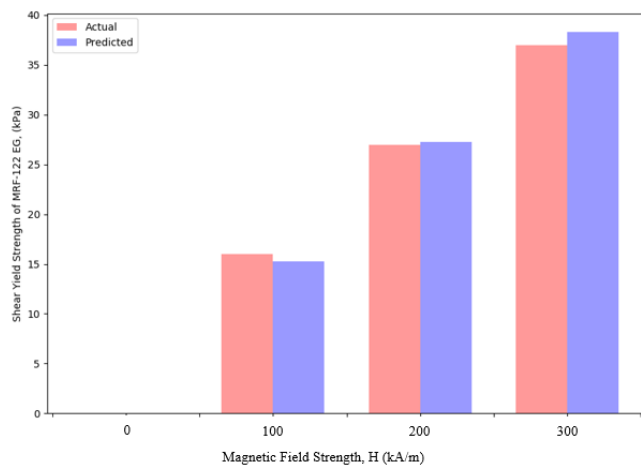

Figure 11. Experimental validation of the model results of shear yield strength against magnetic strength

5. Conclusion

The flow behavior of a magnetorheological fluid in the shear and valve modes for a damper system has been modelled and examined in this paper. Both a pressure-driven flow mode and a direct shear mode were analyzed based on viscoelastic fluid model that is moving between two parallel plates. The momentum equation of the magnetorheological fluid flow was solved using the Laplace transform method to get the velocity and pressure distributions in the unsteady magnetorheological fluid flow between the electrodes of the damper. The solutions of the flow process are simulated, and parametric studies were also provided. The results of the model show an excellent agreement with the experimental results. The viscoelastic flow model describes that the rheological behaviour of the fluid is separated into distinct pre-yield and post-yield regimes. It was established that an increase in the pressure drop enhances the fluid flow velocity, velocity gradient and shear stresses. When the volume fraction of particles increased, the fluid viscosity increases, in consequent, the resistance of the fluid to flow will increase which decreases the fluid flow velocity. The magnetic field intensity increases, the resistance to flow by the magnetorheological fluid increases which in turns decreases the flow velocity of the fluid. Therefore, the present model will be very useful in the design of dampers, shock absorbers, rotary brakes, prosthetic devices, clutches, polishing and grinding devices, etc.

References

Avdeev, M.; Balasoiu, M.; Torok, G.; Bica, D.; Rosta, L.; Aksenov, V.L.; Vekas, L. (2002). SANS study of particle concentration influence on ferrofluid nanostructure. J. Magn. Magn. Mater. 252, 86–88.

Becnel A., Hu W., Wereley N. (2012). Measurement of Magnetorheological Fluid Properties at Shear Rates of up to 25,0001/s. IEEE Trans. Magn. 48:3525–3528.

Chen C I, Chen C K and Yang Y T (2004). Unsteady unidirectional flow of Bingham fluid between parallel plates with different given volume flow rate conditions Appl. Math. Modelling. 28 697–709.

Chen S., Yang J. (2019). Probing Slip Differential Heat of Magnetorheological Fluids Subjected to Shear Mode Operation and Its Effect on the Structure. Materials, 12:1860.

Felicia, L.J.; Philip, J. (2014). Probing of field-induced structures and their dynamics in ferrofluids using sscillatory rheology. Langmuir 30, 12171–12179.

Gedik, E. (2017). Experimental investigation of magnetohydrodynamic flow in circular pipes and numerical analysis with computational fluid dynamics. *Journal of Applied Fluid Mechanics*, *10*, 801–811.

GoldaszJ.S.B.(2012). Nondimensional characterization of flow-mode magnetorheological/electrorheological fluid dampers. *Journal of Intelligent Material Systems and Structures*, *23*, 1545–1562.

Gurubasavaraju, M, Kumar, H, Mahalingam, A. (2018). An approach for characterizing twin-tube shear-mode magnetorheological damper through coupled FE and CFD analysis. *Journal of the Brazilian Society of Mechanical Sciences and Engineering*, *40 (3)*, 1–14.

Huang, H, Sun, S., Chen, S. A. (2019). Numerical and experimental studies on a new variable stiffness and damping magnetorheological fluid damper. *Journal of Intelligent Material Systems and Structures*, *30 (11)*, 1639–1652.

Lee D Y, Choi Y T and Wereley N M (2002). A performance analysis of ER/MR impact damper systems using Herschel–Bulkley model J. Intell. Mater. Syst. Struct. 13 525–31.

Li, Z.; Li, D.; Hao, D.; Cheng, Y. (2017). Study on the creep and recovery behaviors of ferrofluids. Smart Mater. Struct. 26, 105022.

Liao, D. H. W. and W. H. (2011). Magnetorheological Fluid Dampers: A Review of Parametric Modelling. *Smart Materials and Structures*, *20*, 01–34.

Lindler J., Wereley N. (2003). Quasi-steady Bingham plastic analysis of an electrorheological flow mode bypass damper with piston bleed. Smart Mater. Struct. 12:305.

Melzner, K.; Odenbach, S. (2002). Investigation of the Weissenberg effect in ferrofluids under microgravity conditions. J. Magn. Magn. Mater. 252, 250–252.

Omidbeygi F, H. S. (2012). Experimental study and CFD simulation of rotational eccentric cylinder in a magnetorheological fluid. *Journal of Magnetism and Magnetic Materials*, *324*, 2062–2069.

Stepanov G.V., Abramchuk S.S., Grishin D.A., Nikitin L.V., Kramarenko E.Y., Khokhlov A.R. (2007). Effect of a Homogeneous Magnetic Field on the Viscoelastic Behavior of Magnetic Elastomers. Polymer. 48:488–495.

Wang X J and Gordaninejad F (2007). Flow analysis and modeling of field-controllable, electro- and magneto-rheological fluid dampers Trans. ASME J. Appl. Mech. 74 13–22.

Wang, X., & Gordaninejad, F. (2006). Study of magnetorheological fluids at high shear rates. *Rheologica Acta*, *45*, 899–908.

Weiss KD, Carlson JD, Nixon DA. Viscoelastic Properties of Magneto- and Electro-Rheological Fluids. *Journal of Intelligent Material Systems and Structures*. 1994;5(6):772-775.

Yang, Chuncheng, Teng Li, Xiangyu Pei, Jiaxin Li, Zhao Yuan, Yan Li, and Xiufang Bian. (2023). "Magnetorheological and Viscoelastic Behaviors in an Fe-Based Amorphous Magnetic Fluid" *Materials* 16, 5: 1967.